IEEE Access
Multidisciplinary | Rapid Review | Open Access Journal

Received February 2, 2022, accepted February 15, 2022, date of publication February 17, 2022, date of current version March 2, 2022.

Digital Object Identifier 10.1109/ACCESS.2022.3152554

Experimental Analysis of Spatial Modulation Systems in Mixed LOS/NLOS Scenarios

YANNI ZHOU, (Associate Member, IEEE), FLORIN DORU HUTU, (Senior Member, IEEE), AND GUILLAUME VILLEMAUD, (Senior Member, IEEE)

CITI Laboratory, Université de Lyon, INSA-Lyon, 69621 Villeurbanne, France
INRIA, 69621 Villeurbanne, France

Corresponding author: Yanni Zhou (yanni.zhou@insa-lyon.fr)

ABSTRACT Spatial modulation (SM) as a multiple-input multiple-output (MIMO) technique is a solution suitable which offers, with low system complexity and cost, improved spectral efficiency compared to single-input-single-output (SISO) systems. Moreover, the transmission chain is simplified which decreases energy consumption. This paper aims to analyze the SM system transmission under different line-of-sight/non-line-of-sight (LOS/NLOS) propagation scenarios. The analysis of the SM system performance is based on both simulations and experimental results and the bit error rate (BER) is tackled. Concerning the experimental results, two strategies are considered in order to configure the propagation channel. One method consists in constructing a controlled propagation environment. More precisely, the multipath channel's Rician K-factor is imposed by configuring the power levels of the LOS and of the NLOS components. The second method consists in performing over-the-air transmissions on a realistic propagation channel. A channel sounding method allows us to measure the channel characteristics. The experimental results are confronted with the system-level simulation results, good agreement between experimental and simulation results are obtained. The results show that the SM system can maintain the performance in multipath propagation in the presence of indirect paths for both two proposed propagation environments.

INDEX TERMS Spatial modulation, channel sounding, MIMO systems, radio frequency, line-of-sight, non-line-of-sight, experimental results.

I. INTRODUCTION

In recent years, index modulation techniques have exhibited great potential in the scenarios foreseen in next-generation wireless networks [1]. More specifically, spatial modulation (SM) as a single radio-frequency (RF) multiple-input–multiple-output (MIMO) solution has attracted wide attention [2]. SM systems have only one transmitting antenna activated for each time slot. Consequently, the energy consumption assigned to the RF front-end part is reduced because only one RF chain is necessary. SM systems combine modulation on spatial resources with conventional complex modulation. In this way, it exploits the index of the transmitting antennas to convey additional information bits. With these distinctive characteristics, compared to the traditional MIMO systems, SM systems can avoid inter-channel interference, inter-antenna symbol synchronization, and high complexity of detection. Hence, due to the introduction of space resources, SM is a low-cost, low-complexity and high throughput MIMO solution.

SM has also shown promising potential and compatibility in emerging fields. Nowadays, as millimeter-wave (mmWave) and terahertz (THz) communications have triggered widespread interest both in the academic and industrial fields, SM can also guarantee its energy-efficiency characteristic even with a higher free space path loss [3]–[5]. Meanwhile, SM caters to the core issue of cost-saving and energy consumption reduction for smart society, which is considered to be particularly appropriate for application to Internet of Things (IoT) and Internet of Everything (IoE) in [6]–[8].

A comprehensive review and the design guidelines of SM are discussed in [9], [10]. Based on SM, a series of derivative designs of transmitters emerged. The three typical derivative techniques are space shift keying (SSK), quadrature spatial modulation (QSM) and generalized spatial modulation (GSM). From the perspective of reducing system complexity, SSK technique was proposed in [11]. In SSK systems, it is the antenna index used during transmission that relays

The associate editor coordinating the review of this manuscript and approving it for publication was Barbara Masini.

information, rather than the transmitted symbols themselves. QSM has been proposed in [12] in order to improve diversity, which utilizes the orthogonal characteristics of the real part and the imaginary part of the signal and improve the diversity gain by independently selecting the antenna to transmit the real part and the imaginary part. GSM uses index and amplitude/phase modulation signals to transmit information at the same time, and extend the number of activated transmitting antennas from one to multiple [13]. Our research focuses on conventional 2×2 SM systems, part of it is due to the hardware limitation, and the other part is that we mainly analyze the impact of hardware and channel environment on SM system performance.

The performance of the SM system has been shown in [14] while assuming the channel state information (CSI) can be perfectly obtained at the receiving end. The detection of the SM system includes both the detection of the symbols and of the antenna index, so the accuracy of channel estimation plays an important role in the system performance [15]. Several authors [16]–[18] have studied the performance of SM systems in the presence of imperfect channel estimation. However, most of these works are built on a simple channel model, i.e. the classical additive white Gaussian noise (AWGN) model.

Recently, authors of [19], [20] have presented the performance analysis over the more complex channel models by assuming that perfect knowledge of CSI is available at the receiving side. As the perfect CSI is difficult to achieve especially in scenarios with mobility, the CSI estimation errors should be taken into account while evaluating the system performance. In [16], the authors have analyzed the performance of SM in the presence of channel estimation errors by introducing different variances of the estimation errors. The performance of a SM system with a time-varying CSI detector is studied in [21].

Although the theoretical analysis and simulation study of SM is global and in-depth, the experiments on SM are very limited. Because the SM system requires not only traditional symbol demodulation at the receiver side, but also needs the estimation of the information bit encoded by the transmitting antenna which is based on CSI, it is especially important to study the performance of SM in more complex channel environments and realistic scenarios. The performance of the SM system by using measured realistic channels is discussed for the first time in [22]. The idea is to simulate the measured urban correlated and uncorrelated Rayleigh fading channels, then the channel measurements are used to analyse the performance of the SM system. However, the RF parts and the propagation environment are still at simulation level in this work. The following implementations [4], [23] have made up for this lack but the propagation environment is a simple LOS channel. In the recent two years, authors of [24] investigates the BER performance of the SM-OFDM system, with the modified indoor environment simulated in [22]. Besides, first hardware implementation of a SSK system is analyzed in [25]. Here it was shown that the experimental results align closely with simulated ones under a Rician channel with $K = 2.5$. This confirms the feasibility of SSK implementation in an over-the-air environment, but the channel model is relatively simple. Moreover, SSK only needs to detect the switching state and does not transmit the constellation symbols, so the hardware and detection complexity is smaller compared to SM. Recently, a further experimental study of SM system by using a reconfigurable splitting antenna which is capable of selecting one radiation pattern between eight possible configurations has been demonstrated in [26]. The propagation environment in this work can be seen as a short-range direct channel. The above are the results of hardware experimentation related to SM technology nowadays. To the best of the authors' knowledge, there is no previous work considering a realistic indoor propagation environment for the SM system performance evaluation. Therefore, the authors are dedicated to explore the performance of SM systems in real-world channels rather than building simulated channel models.

In this paper, the performance of SM systems is investigated with an experimental testbed in the mixed line-of-sight/non-line-of-sight (LOS/NLOS) environments. The proportion of LOS and NLOS components is evaluated by the Rician K-Factor. Two methods are employed to perform this study. The first one consists in combining the outputs of two SM sources which emulate the direct and complementary paths. The resulting signal is conveyed to the receiver by cable in order to have a precise tuning of the LOS/NLOS communication paths in terms of amplitude and phase. The second method consists in the implementation of an over-the-air transmission scenario in the indoor environment. In order to vary the characteristics of the propagation channel, electromagnetic absorbers are inserted between the emitting and the receiving antennas to modify the power level of the LOS signal. A channel sounding method is also applied to evaluate the characteristics of the propagation channel. The performance of the SM system in the practical implementation is compared to the simulation results. A comprehensive presentation of the simulation framework used by the authors is given in [21].

The main contributions in this work are summarized as follows:

- We conduct experiments on SM systems based on the National Instruments (NI) vector signal transceiver (VST) and LabVIEW programming environment, with the construction of the complete experimental platform and the synchronization of each PXI VST module.
- We introduce two methods (controlled propagation channel and over-the-air propagation channel) to vary the propagation environment. For the real-world indoor propagation environment, a channel sounding approach is applied in order to measure the CSI under different scenarios.
- We identify the transmitting antenna and the symbol by a low-complexity maximum likelihood (ML) detector. Under three typical mixed LOS/NLOS propagation environments, the simulation results concerning

the BER performance are verified by the experimental implementation.

The rest of this paper is divided as follows: in Section II, the step-by-step operations for the transmitting and receiving parts of the SM system are introduced. Section III presents the hardware setup together with the implementation of the two propagation environments. Section IV gives the system performance obtained by the proposed experimental testbed in the mixed LOS/NLOS scenarios. Furthermore, the results are compared with those obtained by simulations. Finally, Section V concludes this paper and gives some future directions for this work.

II. TRANSMITTING AND RECEIVING PROCESSES OF THE SM SYSTEM

The experiment setup can be divided into software and hardware parts, from simulation level and from physical level, respectively. The block functions and the transmission chain are given in FIGURE 1. The SM system is implemented by using four NI PXIe-5646 VST modules [27] which are programmed by using NI LabVIEW framework. The VST as a vector signal transceiver is able to transmit and to receive at the same time and at the same frequency. Here, to realize a 2×2 SM system, two VST modules are supposed to work for the emission and the remaining two modules are employed for the reception. The four VST modules are integrated into a PXIe chassis which can guarantee the symbol synchronization by configuring the synchronization function. More details on the hardware setup will be presented in Section IV.

This section presents the software part of the proposed 2×2 SM system. On the generation side, the software programs aims at selecting the bits dedicated to forming digital modulation symbols and the bits dedicated to switching between the transmitting VST modules from the input bitstream. This switching between the two VST's corresponds to the antenna switching in a realistic ''SM'' implementation. In our case, the quadrature phase-shift keying (QPSK) as a digital modulation method is employed. Then, the signal generated by the transmitting VST modules passes through the propagation channel (imposed or over-the-air). The signal received by the VST modules is processed in order to identify the transmitting antenna and to demodulate the QPSK symbols. The VST modules are driven by LabVIEW which is coupled with Matlab software. This latter software is employed to implement the complex signal processing algorithms (i.e. maximum likelihood (ML) optimal detection algorithm, least-square (LS) algorithm) in the step of the SM modulation, channel estimation and SM demodulation.

A. TRANSMITTING PART

FIGURE 2 outlines the step-by-step configuration of the transmitting part. The input data is a random bitstream which will be processed by the SM mapping algorithm. In order to configure the parameters (carrier frequency, modulation type, power level, etc.) of the VST modules, NI-RFSG libraries provided by LabVIEW software are employed. More precisely, NI-RFSG is an instrument driver which is able to configure and operate hardware, to program and generate signals, and to perform modulation tasks using LabVIEW VIs functions [28]. In the following, the main signal processing steps are detailed.

1) CONFIGURATION

Once the NI-RFSG session is opened, the carrier frequency and the output power level are configured. The carrier frequency is set up at 868 MHz (inside one of the European ISM band), which is chosen in order to comply with our hardware constraints (VST platform, frequency synthesizer, phase coherent coaxial cables, antennas, etc.) and simulation capabilities. The output power level can be adjusted as required in the limit range of the VST and the regulations which will be introduced in the following sections. We then configure the generation mode and the reference clock source. The RF signal generator has also been configured to be able to generate an arbitrary waveform. The reference clock source must be external to the device and we apply the sampled reference clock (SRC) for the synchronization of four VST modules.

2) DAISY CHAINED LOCAL OSCILLATORS (LO)

For the four VST emulating a 2×2 SM transmission, the LO's are supplied by an external source (RF frequency synthesizer) coupled to a 1:4 power divider. Otherwise, another option is to setup the LO's of the four VST modules in a ''daisy chain'' configuration. An external LO source is applied for our SM system. Firstly, we define the VST corresponding to the antenna index 1 as master device and the VST corresponding to the antenna index 2 as slave device. Moreover, the two VST modules employed at the reception are also set up as slave device. The four VST modules are configured in order to receive the LO from an external source, at the LO input terminals. The employed external source is a configurable frequency synthesizer. The signal provided by the frequency synthesizer is dispatched to the four VST modules through a 1:4 RF power divider. The coaxial cables are employed to connect the LO inputs of the VST modules to the outputs of the power divider. However, coaxial cables insert different phase shifts, a prior correction is performed in order to guarantee the phase coherence. In general, we always need to ensure that the up-converter center frequencies match on all devices when sharing LOs. Even if the carrier frequency is a multiple of the LO frequency step size, there may be a small amount of LO frequency offset due to the limited resolution of the phase-locked loop (PLL) fractional mode dividers. In our particular case, the VST modules are configured in order to perform a direct conversion. Consequently, both for the emission and for the reception, the intermediate frequency is equal to zero.

3) SYNCHRONIZATION

To perform SM, the symbol synchronization needs to be configured. For the implementation of the synchronization,

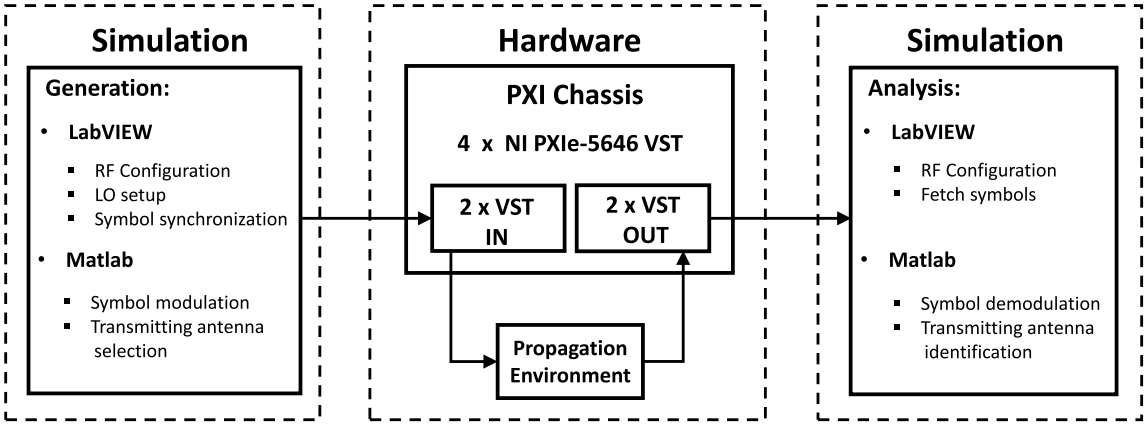

FIGURE 1. Main parts of the experimental setup.

one of the VST modules takes the role of master and dispatches the clock signal towards the remaining VST modules. The start trigger synchronization should be first configured. Among the applied four VST modules in our system, it is the master device who drives the trigger distribution line. It must be configured to be master for the synchronized sample clock, and a synchronized sample clock distribution terminal must be arranged. For the slave device, the trigger distribution terminal is given. The slave device uses the trigger distribution signal to generate the "sync-start" signal. As done for the master device, an additional step is required to ensure synchronization that a synchronized sample clock distribution terminal must be configured. Moreover, the slave device should be triggered on the rising edge of the "sync-start" signal. Noteworthy, a prior configuration of the trigger bus line need to be done by NI MAX. Basically, whichever module is providing the sample clock, look at what slot it is in, and connect the trigger buses in MAX so that triggers are routed away from that trigger bus.

4) SM MODULATION

As mentioned before, the input will be processed by the SM mapping algorithm which is given in FIGURE 3. In our case, we have two transmitting antennas ($N_t = 2$) and QPSK ($M = 4$) is chosen as the modulation method. As there are four possible symbols for the QPSK modulation, each possible 3-digit ($\log_2(N_t) + \log_2(M) = 3$) binary represents one possible transmitting situation of the SM system. Moreover, P ($P = N_t M = 8$) is given to denote the number of possible configurations of the SM. As a header, additional 8 ($P = N_t M = 8$) frames of data are added before the random input sequence. This header is employed in order to estimate the propagation channel characteristics (i.e. CSI), which is used at the receiver side for SM demodulation. As shown in the right part of FIGURE 2, the input signals for the two transmitting VST modules need to be prepared. According to the input bitstream, four sets of I and Q values for the master and slave devices are generated.

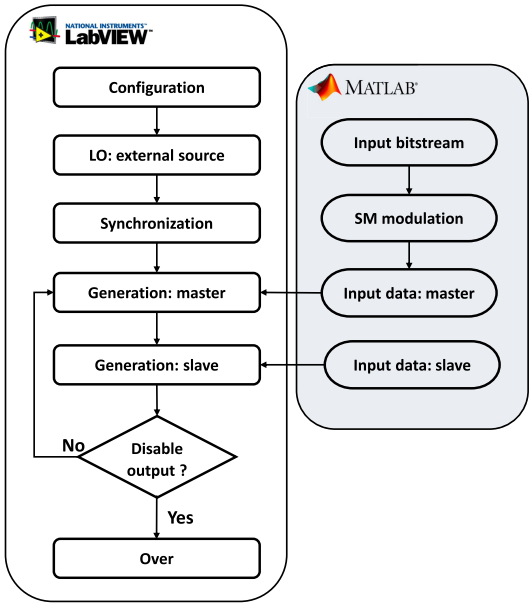

FIGURE 2. A step-by-step process of the SM transmitting part.

5) GENERATION

The two VST modules for the transmission will generate the IQ samples based on the given input, one at a time, with the carrier frequecy of 868 MHz and input power of −20 dBm. The generation is performed continuously, until it is manually stopped. Finally, the outputs of the VST modules are disabled and the NI-RFSG session is closed.

B. RECEIVING PART

The step-by-step operations of the receiving part are shown in FIGURE 4. This part analyzes the received signal in order to recover the input bitstream. In addition, the bitstream employed at the transmitting part is compared to the one recovered at the receiving part and the bit error rate (BER) is calculated. The configuration of the receiving end is performed by using NI-RFSA session in the LabVIEW programming environment. In general, NI-RFSA is an instrument

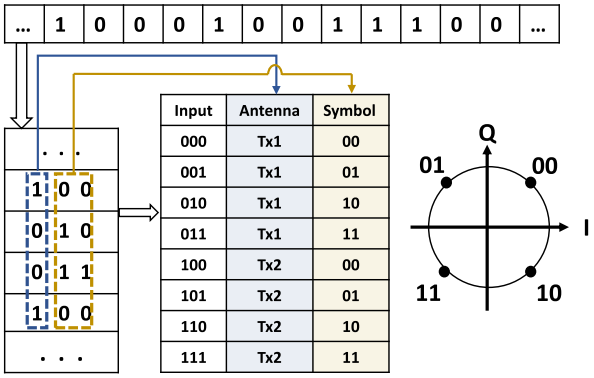

FIGURE 3. SM mapping algorithm for $N_t = 2$ and QPSK modulation.

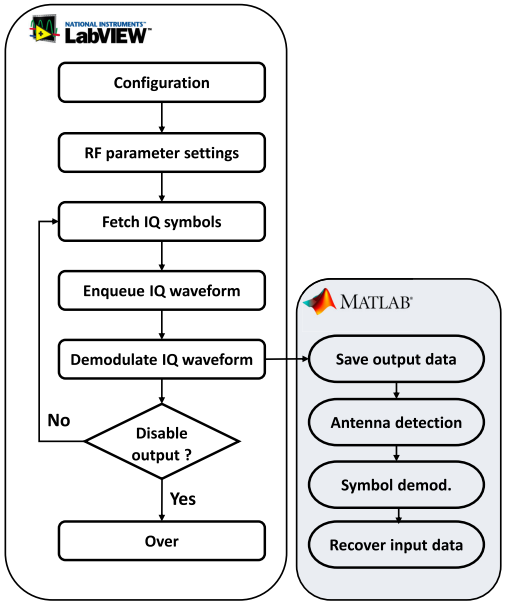

FIGURE 4. A step-by-step process of the SM reception part.

driver to control and configure NI's vector signal analyzers (VSA) [29]. It provides a set of operations and properties which allow the creation of custom metrics or applications that require IQ data. A step-by-step process of the receiving end is described in detail thereafter:

1) CONFIGURATION

Once the NI-RFSA session is initialized, we configure IQ acquisition, carrier frequency, reference level and symbol rate for acquisition. The reference level represents the maximum expected power of an input RF signal.

2) RF PARAMETER SETTINGS

For the following demodulation, QAM system parameters (e.g. modulation order, symbol map, etc.) are configured firstly, then we generate the matched filter coefficients for pulse-shaping and matched filters applied by the digital demodulation. The raised cosine filter is applied and the roll-off factor is set at 0.5. Moreover, a synchronization parameter cluster should be constructed. The generated synchronization parameter cluster guarantees that the different symbols which come from the two VST's configured in the receiving part, are received according to the same time base.

3) FETCH AND ENQUEUE IQ WAVEFORM

After transposing the received signals into BB, the different complex samples generated by the transmitting VST modules are fetched. The producer loop and the consumer loop are constructed. They are employed to fetch and process IQ samples. The producer/consumer model enables two processes to work at the same time, so that for the receiving end, the received signals can be demodulated continuously. We enqueue the IQ waveform acquired in the producer loop and dequeue the IQ waveform in the consumer loop. Next, the input complex-valued waveform is sampled and adjusted to the required IQ rate. Additionally, the number of samples fed into the QPSK demodulation should correspond to an integer number of symbols.

4) QPSK DEMODULATION

The demodulation as the core step in the RFSA module, Matlab software is introduced to perform the LS algorithm and the ML algorithm. The LS algorithm is a traditional and effective method for CSI estimation, which has already been demonstrated in [21] for the simulation implementation of the SM system. The constellation of the received symbols is shown in FIGURE 5. We suppose here Tx1 and Tx2 as the two transmitting antennas. One can remark from the FIGURE 5 that the two QPSK constellations of the signal transmitted by Tx1 and Tx2 are different in terms of amplitude, and a slight rotation between the two constellations is also visible, since the transmission channels between the two transmitting antennas and the receiving ones are quite different.

IQ data waveform for the constellation at the receiving end is shown in FIGURE 6. The scale-like part represents the demodulation result of the P frames of the header. Because the demodulation process is a continuous loop, the header part just follows the previous set of random signals in FIGURE 6.

The basis of SM demodulation is to estimate the CSI of the different channels, and then the symbols and the transmitting antenna index can be detected according to the estimated CSI. More precisely, P frames of data as a header of the transmitted bitstream is prepared for the CSI estimation. The principle of the CSI estimation is based on LS algorithm. Every M frames of the incoming header can get Nr channel states, the total P frames allow us to obtain the channel matrix $\mathbf{H}$, where $\mathbf{H} \in \mathbb{C}^{N_r \times N_t}$. The propagation channel is supposed as an indoor one which is modeled as a Rician fading channel. Here, N_r is the number of the receiving antennas. The Rician fading channel model $\mathbf{H}$ takes into account the presence of the LOS path and the scattered NLOS paths, the proportion of LOS and NLOS paths are evaluated by the Rician K-factor. More precisely, the Rician K-factor is defined as the ratio between the main signal power (usually the LOS path

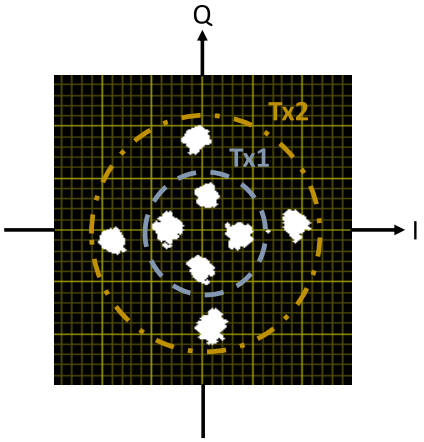

FIGURE 5. Constellation of the received SM signal.

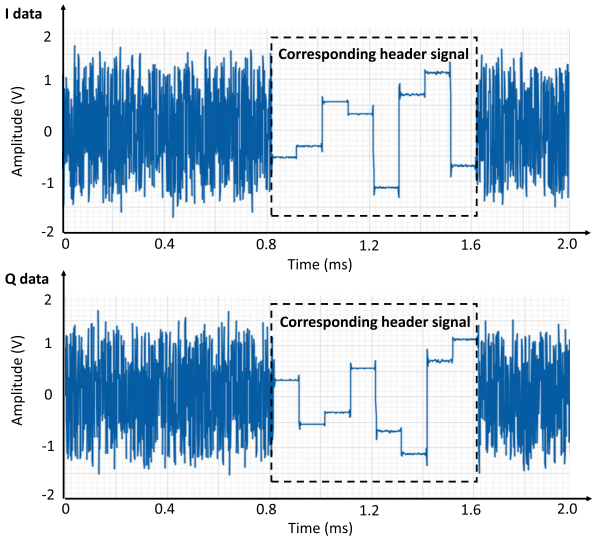

FIGURE 6. The constellation data of the I and Q branches at the receiving end.

signal) and the sum of the remaining multipath (NLOS paths) powers. In this particular case, $\mathbf{H}$ has the following structure:

$$\mathbf{H} = \sqrt{\frac{K}{K+1}} \cdot \mathbf{A} + \sqrt{\frac{1}{K+1}} \cdot \mathbf{V} \tag{1}$$

where $\mathbf{A}$ is a deterministic matrix and $\mathbf{V}$ is a stochastic one.

Additionally, we can increase the accuracy of the estimation by increasing the length of the header, we suppose that the number of symbols for each frame is N_h.

The structure of the header $\mathbf{A}^*$ is given by the following equation:

$$\mathbf{A}^* = \begin{bmatrix} \underbrace{a_1 \cdots a_1}_{N_h} \\ \underbrace{a_2 \cdots a_2}_{N_h} \\ \vdots \\ \underbrace{a_P \cdots a_P}_{N_h} \end{bmatrix}^{\mathbf{T}} \tag{2}$$

Therefore, the composition of each frame $\mathbf{A}_p^*$ can be presented as equation (3):

$$\mathbf{A}_p^* = \left[a_p^1, a_p^2, \cdots, a_p^{N_h}\right] \tag{3}$$

where $a_p^{n_h}$ denotes one of the P possible symbols transmitted by N_t antennas of the SM modulation. $\hat{\mathbf{w}}$ is assumed as the calculated complex-valued coefficient matrix, which denotes the relation between input signals in the header and the received signal at the receiving part.

$$\hat{\mathbf{w}} \overset{\text{def}}{=} \left[\hat{w}_1 \quad \hat{w}_2 \cdots \hat{w}_P\right] \tag{4}$$

The received signal matrix $\mathbf{y}^*$ for this frame is presented as:

$$\begin{aligned} \mathbf{y}^* &\overset{\text{def}}{=} \left[\mathbf{y}_1 \quad \mathbf{y}_2 \quad \cdots \quad \mathbf{y}_P\right] \\ \mathbf{y}_p^* &= \left[y_p^1, y_p^2, \cdots, y_p^{N_h}\right] \end{aligned} \tag{5}$$

Then, we can obtain the component $\hat{w}_p$ in $\hat{\mathbf{w}}$ according to the LS algorithm:

$$\hat{w}_p^{LS} = \arg\min_{w} \left\| \mathbf{y}_p - \hat{w}_p \cdot \mathbf{A}_p^* \right\|^2 \tag{6}$$

$$\hat{w}_p^{LS} = \left(\mathbf{A}_p^{*H} \cdot \mathbf{A}_p^*\right)^{-1} \cdot \mathbf{A}_p^{*H} \cdot \mathbf{y}_p^* \tag{7}$$

where the operator $[\,\cdot\,]^H$ represents the Hermitian transpose. Once we estimated the CSI, more precisely, the amplitude and phase deformation for the P possible symbols transmitted by N_t antennas, the necessary information for the detection is ready. For each input signal, a correction of the channel model is performed by using the obtained P components $\hat{w}_p^{LS}$ in the coefficient matrix $\hat{\mathbf{w}}$ to recover the input signal.

Then, the ML optimal detection algorithm is applied for index demodulation of the transmitting antenna and the modulated symbols [30]. A low-complexity ML detector is considered, by using the phase difference of different symbols in QPSK. Here, we suppose the initial phase of the QPSK modulation is $\pi/4$, then the symbol $s_n$in this constellation can be expressed as:

$$s_n = A\left[\cos(\varphi_n) + j\sin(\varphi_n)\right] \quad n = 1, 2, 3, 4 \tag{8}$$

where A is the amplitude of the symbol, and $\varphi_n = (2n-1)\frac{\pi}{4}$. $\hat{n_t}$, $\hat{s}$ are assumed as the estimated activated antenna index and transmitted symbol respectively. Then, we can obtain by ML algorithm:

$$\begin{aligned} (\hat{n_t}, \hat{s})_{ML} &= \arg \min_{n_t \in \mathbf{N_t},\, s \in \mathbf{S}} \left(\|\mathbf{yw} - s\|^2 \right) \\ \mathbf{S} &= \{s_1,\ s_2,\ s_3,\ s_4\} \\ \mathbf{N_t} &= \{1,\ 2,\ \ldots,\ N_t\} \end{aligned} \tag{9}$$

The demodulation can be divided into two steps. Firstly, the index of transmitting antenna is detected. Here, an example of SM constellation is given in FIGURE 7. To simplify the comprehension, we employ $N_t = 2$ and no phase shift between the two transmitting antennas. The inner and outer circle symbols can be considered as transmitted by Tx1 and Tx2, respectively.

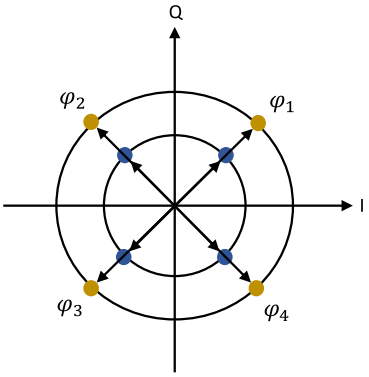

FIGURE 7. Constellation of SM modulation with QPSK and $N_t = 2$ (no phase shift).

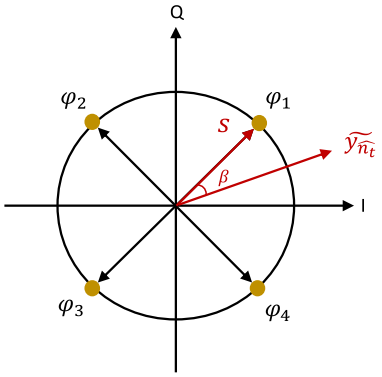

FIGURE 8. ML detection method for QPSK symbols.

One can remark that the same amplitude of the four symbol points can be obtained for the same transmitting antenna. Therefore, the detection of antenna index can be simplified as the optimization of amplitude.

$$(\hat{n}_t)_{ML} = \arg \min_{n_t \in \mathbf{N_t}} (|\mathbf{yw}|^2 - |s|^2) \tag{10}$$

The estimated index of transmitting antenna is denoted by $\hat{n}_t$. Then, the optimization issue $(\hat{s})_{ML} = \arg\min_{s\in\mathbf{S}} \left(\|\mathbf{yw} - s\|_2^2\right)$ can be written as:

$$(\hat{s})_{ML} = \arg \min_{s\in\mathbf{S}} \left(\left|\tilde{y}_{\hat{n}_t} - s\right|^2\right) \tag{11}$$

where $\tilde{y}_{\hat{n}_t} = \mathbf{yw}$. $\hat{y}_{\hat{n}_t}$ and s can be denoted as $\tilde{y}_{\hat{n}_t} = r_{\hat{n}_t} e^{j\theta_{\hat{n}_t}}$, $s = e^{j\varphi}$ ($A = 1$ is assumed for simplification) in polar form, then $(\hat{s})_{ML}$ can be expressed as

$$\begin{aligned}
(\hat{s})_{ML} &= \arg \min_{s\in\mathbf{S}} \left(\left|\tilde{y}_{\hat{n}_t} - s\right|^2\right) \\
&= \arg \min_{\varphi\in\Psi} \left|r_{\hat{n}_t} e^{j\theta_{\hat{n}_t}} - e^{j\varphi}\right|^2 \\
&= \arg \min_{\varphi\in\Psi} \left(r_{\hat{n}_t} e^{j\theta_{\hat{n}_t}} - e^{j\varphi}\right)\overline{\left(r_{\hat{n}_t} e^{j\theta_{\hat{n}_t}} - e^{j\varphi}\right)} \\
&= \arg \min_{\varphi\in\Psi} \left(\left|r_{\hat{n}_t}\right|^2 + 1 - 2r_{\hat{n}_t} \cos\left(\theta_{\hat{n}_t} - \varphi\right)\right) \\
\Psi &= \{\varphi_1,\ \varphi_2,\ \varphi_3,\ \varphi_4\}
\end{aligned} \tag{12}$$

If the $\hat{n}_t$ is firstly detected, the optimization of the symbol has the form as follows:

$$\begin{aligned}
(\hat{\varphi})_{ML} &= \arg \max_{\varphi\in\Psi} \left(\cos\left(\theta_{\hat{n}_t} - \varphi\right)\right) \\
0 \le \theta_{\hat{n}_t} &< 2\pi, \quad 0 \le \varphi < 2\pi
\end{aligned} \tag{13}$$

We can conclude that $0 \le \left|\theta_{\hat{n}_t} - \varphi\right| < 2\pi$. This optimization can be divided into two cases:

For $0 \le \left|\theta_{\hat{n}_t} - \varphi\right| < \pi$:

$$(\hat{\varphi})_{ML} = \arg \min_{\varphi\in\Psi} \left|\theta_{\hat{n}_t} - \varphi\right| \tag{14}$$

For $\pi \le \left|\theta_{\hat{n}_t} - \varphi\right| < 2\pi$:

$$(\hat{\varphi})_{ML} = \arg \max_{\varphi\in\Psi} \left|\theta_{\hat{n}_t} - \varphi\right| \tag{15}$$

The principle of ML method to detect QPSK symbol can be explained in FIGURE 8. Here, β is assumed as the difference between $\theta_{\hat{n}_t}$ and φ. One can remark that the closer the symbol point s to $\tilde{y}_{\hat{n}_t}$, the smaller value in (12) is. In other words, if the angle β between $\tilde{y}_{\hat{n}_t}$ and s is smaller, then the value of $\cos\left(\theta_{\hat{n}_t} - \varphi\right)$ is larger. Once $\hat{\varphi}$ is estimated, the transmitting QPSK symbol can be directly demodulated.

Therefore, we can conclude the demodulation as follows: (1) Detect transmitting antenna index: the most likely transmitting antenna is the antenna giving the smallest amplitude difference between the received corrected symbol and one of the four QPSK symbols. (2) Estimate digital modulation symbol: because of using the QPSK modulation, only four possible symbols exist. The detection is simplified by calculating the phase difference β. (3) The binary values corresponding to the estimated QPSK symbol are concatenated with the binary values obtained by identifying the emitting antenna to recover the transmitting bitstream.

III. HARDWARE SETUP AND PROPAGATION ENVIRONMENT

A. HARDWARE SETUP

In general, NI PXI platform is designed for measurement and automation applications. It supports high-performance, modular instruments and I/O modules that enable specialized synchronization and critical software functions for test and measurement applications, from hardware validation to production self-testing. As shown in FIGURE 1, the PXI chassis as the hardware assumes the role of transmitting the modulated signals and receiving the signals that have passed though the propagation environment. For our experiments, the NI-PXIe-1085 chassis is equipped with four VST modules of the type PXIe-5646R. FIGURE 9 shows a photograph of the PXIe-5646R modules fitting into the NI-PXIe-1085 chassis for the application of our SM system.

The PXIe-1085 Chassis has 16 hybrid slots and incorporates all the features of the PXI specifications, including support for PXI modules with a built-in 10 MHz reference clock, a PXI trigger bus, and a PXI star trigger. Each slot equipped with a VST module in the chassis has the capability of both transmitting and receiving signals by configuring the inputs and the outputs.

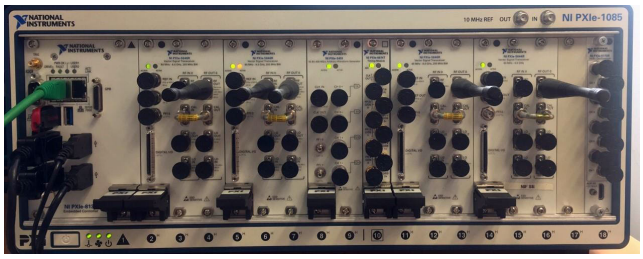

FIGURE 9. NI PXIe-1085 chassis containing four PXIe-5646R VST modules.

The NI PXIe-5646R RF VST module combines the typical RF I/O functions of vector signal analyzer (VSA) and vector signal generator (VSG) with NI or user-defined functions. The PXIe-5646R has the particularity of sharing the internal local oscillator between the emitting and the receiving parts. The RF input and RF output of the PXIe-5646R can operate in a frequency range from 65 MHz to 6 GHz, and have an instantaneous bandwidth of up to 200 MHz. TABLE 1 gives the main parameters of NI PXIe-5646R VST.

B. PROPAGATION ENVIRONMENT

For the practical implementation of the SM system, the indoor environment is considered. Besides the LOS component, there are usually NLOS components which may be caused by the complex propagation environment, for example, the reflection of the emitted signal by the objects between or around the transmitting antennas and the receiving ones. The relation between the output $\mathbf{y}$ and the input $\mathbf{x}$ can be written as follows:

$$\mathbf{y} = \mathbf{H} \cdot \mathbf{x} + \boldsymbol{\eta} \tag{16}$$

$$\mathbf{H} = \begin{bmatrix} h_{1,1} & \cdots & h_{1,N_t} \\ \vdots & \ddots & \vdots \\ h_{N_r,1} & \cdots & h_{N_r,N_t} \end{bmatrix} \tag{17}$$

where the channel matrix $\mathbf{H} \in \mathbb{C}^{N_t \times N_r}$. In our case, $N_t = N_r = 2$. Moreover, an AWGN term η, is considered. The received RF signal $y_{p,q}(t)$ from Tx antenna element p to Rx antenna element q in this case can be written as:

$$y_{p,q}(t) = h_{p,q} \cdot x_{p,q}(t) + \eta \tag{18}$$

The transmitted signal $x_{p,q}(t)$ is assumed to be the modulated QPSK signal within a symbol duration T_{sym}, then it may take the form:

$$x_{p,q}(t) = \cos\left(2\pi f_c t + \theta_n\right), \quad 0 \le t \le T_{sym}, \ n = 1, 2, 3, 4 \tag{19}$$

where the signal phase is given by

$$\theta_n = (2n-1)\frac{\pi}{4} \tag{20}$$

Therefore, the received signal $y_{p,q}(t)$ can be presented:

$$y_{p,q}(t) = D_{LOS} \cdot \cos\left(2\pi f_c t + \theta_n\right) + \sum_{i=1}^{L} a_i \cos\left(2\pi f_c t + \theta_n + \varphi_i\right) + \eta \tag{21}$$

TABLE 1. Main parameters of NI PXIe-5646R VST.

Frequency Range	65 MHz to 6 GHz
Bandwidth	200 MHz
Phase Noise (20 kHz offset) < 3 GHz	-99 dBc/Hz
Absolute Amplitude Accuracy (375 MHz to 2 GHz), 15 °C to 35 °C	± 0.35 dB to ± 0.65 dB
Average Noise Floor Density	-161 dBm/Hz
Maximum Output Power (CW)	+10 dBm
Minimum Output Power	-168 dBm
Modulation Capabilities	Vector Modulation

where D_{LOS} is the amplitude of the direct (LOS) component, f_c represents the carrier frequency. L is the number of NLOS paths. The random variable corresponding to the amplitude of the i^{th} NLOS path signal is denoted by a_i. The inserted phase shift is also considered as a random variable, is denoted φ_i.

With the considered propagation environment, we explore the possibility of the system's performance at different Rician K-factor values and work to verify the simulation results. Therefore, two methods have been proposed to generate the scenarios and calculate the Rician K-factor. The first method consists in generating the defined LOS/NLOS scenarios in a controlled environment (by cable). Hence, the precise variation of the LOS and the NLOS power levels is available. The drawback is that only one NLOS path has been implemented. The other strategy is to configure a realistic, over-the-air indoor environment and to measure the channel coefficients by the channel sounding. Thereafter, the two methods are presented in details.

1) SM TRANSMISSION UNDER A CONTROLLED PROPAGATION ENVIRONMENT

In order to simulate the mixed LOS and NLOS scenarios, it is supposed that there is one direct path and one indirect path, respectively, for each $h_{n_r n_t}$ in the channel matrix $\mathbf{H}$. In this case, L is equal to 1 in equation (21). By definition, we have a Rician K-factor of this multipath:

$$K \triangleq |D_{LOS}|^2 / 2\,|a_1|^2 \tag{22}$$

The experimental scenario of the SM system with one LOS path, one NLOS path and two transmitting antennas ($N_t = 2$) is presented in FIGURE 10. Here, the two LOS paths and the two NLOS paths are emulated by the four VST modules configured as transmitters. The outputs of these four VST modules are gathered by a four-way directional coupler. The resulting signal is transmitted to one of the VST modules which is also configured as the receiver. Four coaxial cables having the same electrical length at 868 MHz have been used between the four VST modules and the divider. Few differences may occur since the phase coherence is not completely respected and, moreover, there are variations in terms of attenuation. Hence, the amplitude and phase errors inserted by the experimental setup are measured and corrected beforehand.

Through this method, we can accurately define the power level of LOS and NLOS components. However, the limitation of this method is obviously that there is only one secondary path.

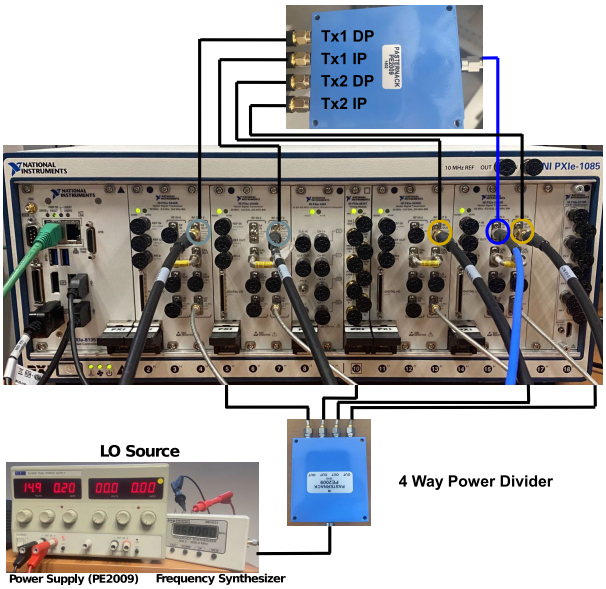

FIGURE 10. Experimental setup of the SM system with controlled propagation environment. In this case, $N_t = 2$ and $N_r = 1$, one LOS path and one NLOS path are configured for each transmitting channel.

2) OVER-THE-AIR SCENARIO

In this case, we are employing omnidirectional antennas to transmit and receive signals, where their electrical and radiation characteristics are similar and they are placed at the same height. The separation distance is set to one and a half wavelengths. A picture of the experimental setup implemented for the study of 2×2 SM system is presented in FIGURE 11. Due to our limited indoor area and distance between the transmitting and the receiving antennas, the LOS signal is predominant. In order to bring more complexity (i. e. decrease the K factor), electromagnetic absorbers are placed between the transmitting and the receiving antennas.

In this over-the-air scenario, the channel characteristics are not known in advance. In order to overcome this problem, a channel sounding strategy has been implemented.

The theoretical realization method of the channel sounding is described in [31]. Generally, in a time-varying multipath channel, because of its stochastic behavior, a statistical model may be established and a power delay profile may be introduced. Power delay profile, also called multipath intensity profile, represents the average relative power as a function of the relative delay of the NLOS paths and it can be measured empirically. By calculating the channel's impulse response, it is possible to obtain the power delay profile and to extract parameters like the mean excess delay (i.e. the first moment of the power delay profile), the root mean square (RMS) delay spread (i.e. the square root of the second central moment of the power delay profile). Moreover, the number of the paths can be determined by properly choosing a power level threshold.

The temporal variation of the channel's model have a corresponding relationship on the temporal variation of the impulse response's multipath components. The channel's output $y(t)$ is found by the convolution between the channel's impulse response $h(t, \tau)$ and its input $x(t)$. Here, the single-input-single-output (SISO) case is introduced to present the channel detection method.

$$\mathrm{y(t)} = \mathrm{h(t,}\ \tau) * x(t) = \int_{-\infty}^{\infty} \mathrm{h(t,}\ \tau) x(t-\tau) d\tau \tag{23}$$

where $*$ denotes the convolution operator and τ corresponds to the delay. The model of a wireless channel can be represented by

$$h(\mathrm{t},\ \tau) = \sum_{i=1}^{L} \propto_i (t) \cdot \delta\,(t - \tau_i)\, e^{j\varphi_{i(t)}} \tag{24}$$

where L is the number of different propagation paths; $\propto_i$ is modeled as a random coefficient with a certain probability density function; the Dirac delta function is denoted by δ; τ_i represents the delay of the L multipaths.

In order to determine the channel's model, the core idea is to use the good correlation property of pseudo noise (PN) sequences [32]. Indeed, a PN sequence has been transmitted through the wireless propagation channel, and then the received response is correlated with it in order to calculate the channel coefficients. Assuming that a long-length repetitive PN sequence is transmitted, the channel response is matched and filtered at the receiver. For the impulse testing systems, it is difficult to maintain a uniform spectral density across the entire bandwidth using a single impulse. In this way, impulses with low power levels may be masked by noise, or impulses with high power levels may produce an overload of the receiver stage. Using the uniform energy spectrum over the bandwidth of the PN sequence, the impulse response of the channel can be determined.

As stated, the principle of this method is to apply a PN sequence as the input signal. The cross-correlation of the reference PN sequence and the received PN sequence is given as follows:

$$\begin{aligned} r_{qy}(\tau) &= \lim_{T\to\infty} \frac{1}{T} \int_0^T q(t)\mathrm{y}(t+\tau) dt \\ &= \lim_{T\to\infty} \frac{1}{T} \int_0^T q(t) dt \int_{-\infty}^{\infty} \beta_h(v) q(t-v+\tau) dv \end{aligned} \tag{25}$$

where $\beta_h(t)$ is the impulse response, $q(t)$ and $\mathrm{y}(t)$ represent the input PN sequence and output signal, respectively.

Since the output of the system $\mathrm{y}(t)$ is the convolution between the input and the impulse response, we can obtain

$$\mathrm{y}(t) = \int_{-\infty}^{\infty} h(v) q(t-v) dv \tag{26}$$

After changing the integration order in the equation (25), we have

$$\begin{aligned} r_{qy}(\tau) &= \int_{-\infty}^{\infty} h(v) dv \lim_{T\to\infty} \frac{1}{T} \int_0^T q(t) q(t-v+\tau) dt \\ &= \int_{-\infty}^{\infty} h(v) r_{qq}(t-v) dv \end{aligned} \tag{27}$$

FIGURE 11. Experimental setup of a 2 × 2 SM system with realistic propagation environment.

The autocorrelation function of the PN sequence (r_{qq}) approximates to a Dirac delta function. Therefore, the cross-correlation can be expressed as

$$r_{qy}(t) = \mathrm{R}\int_{-\infty}^{\infty} h(v)\delta(t-v)dv = \mathrm{R}h(t) \tag{28}$$

where R denotes the surface of the impulse function and it is equal to the RMS value of the noise.

By calculating the correlation function of the PN sequence, the parameters of the transmission channel are estimated. In this way, by using the same setup as for the SM system, a simple wireless transmitter-receiver system has been established in order to perform the channel sounding. The PN sequence is sent by using a simple BPSK modulation. Other parameters as the input signal power and the symbol rate are given in TABLE 2. In this way, the channel coefficients can be measured. The Rician K-factor is calculated by

$$K = 10 \cdot log_{10}\left(\frac{\max\left(\left(\hat{\alpha}_l\right)^2\right)}{\sum_{l=1}^{L}\left(\hat{\alpha}_l\right)^2 - \max\left(\left(\hat{\alpha}_l\right)^2\right)}\right)\ [\mathrm{dB}] \tag{29}$$

where $\hat{\alpha}_1 \in \left\{\hat{\alpha}_1, \hat{\alpha}_2, \cdots, \hat{\alpha}_L\right\}$, are the amplitudes of the different multipaths.

IV. PERFORMANCE EVALUATION OF THE SM SYSTEM

In this section, we discuss the BER performance of the mentioned SM system under the LOS/NLOS scenarios. The two propagation environment scenarios previously described are considered. One is the controlled propagation environment and the other is the realistic channel. Due to the hardware limitation, a simple 2×2 SM scenario has been implemented. To compare with the experimental approaches, a simulator of the SM scheme was built in [21] with the help of the Keysight ADS and Matlab software. Similar to the experimental implementation, in the simulation setup, a time varying CSI detector is applied to estimate the simulated propagation environment, and 10^6 input binary values are transmitted in order to estimate the BER. The parameters of the experimental system are gathered in TABLE 2.

TABLE 2. Parameters of 2 × 2 SM experimental setup.

Parameter	Value
Carrier frequency	868 MHz
Tx number (N_t)	2
Rx number (N_r)	2
Modulation type	QPSK
Symbol rate	10 Mbit/s
Output sample time step	0.1 us
Input signal power	-10 dBm
Total number of input binary bits (except header)	10^6
Number of symbols of frame for CSI estimation	10^3
PN sequence order for channel sounding	11
Modulation type for channel sounding	BPSK
Threshold of multipaths (in terms of peak value)	30 dB

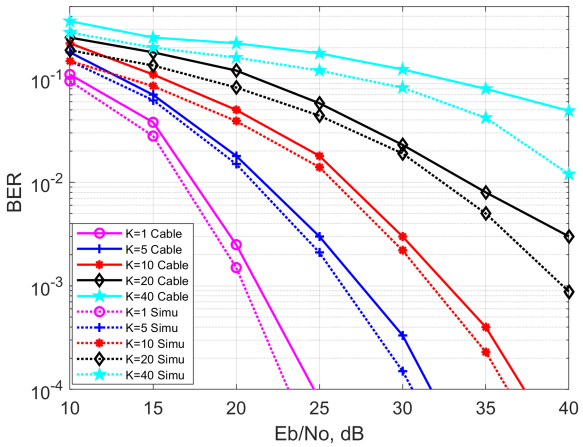

FIGURE 12. Simulation and experimental results with controlled propagation environment for the BER performance of the SM system under mixed LOS/NLOS scenarios.

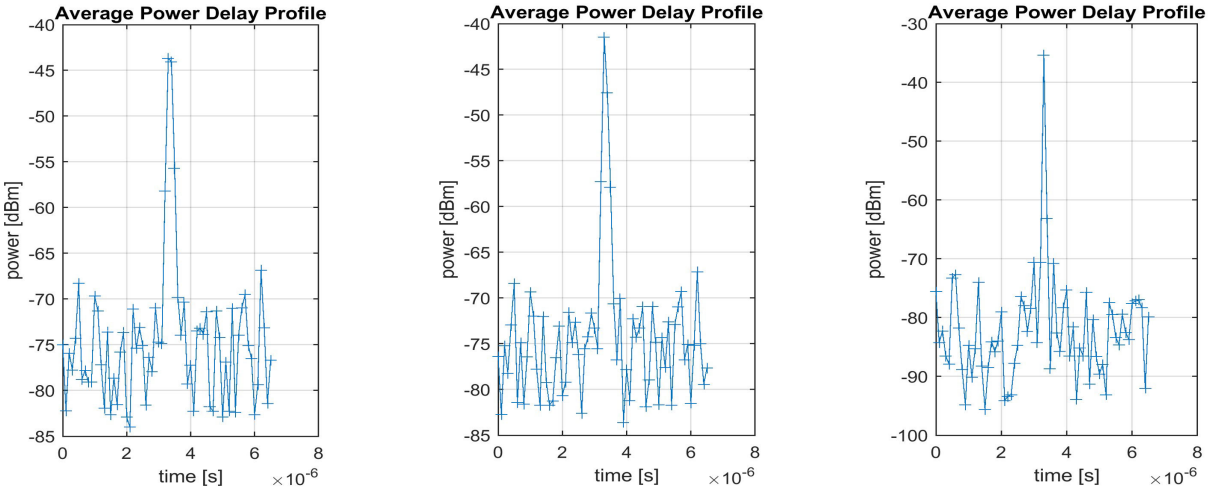

(a) $K = 5.3$ dB (b) $K = 20.1$ dB (c) $K = 39.1$ dB

FIGURE 13. Measured average power delay under $K = 5.3$ dB, 20.1 dB and 39.1 dB.

A. EXPERIMENTAL EVALUATION OF THE SM TRANSMISSION OVER A CONTROLLED PROPAGATION ENVIRONMENT

Firstly, we implement the approach of predefining the propagation environment which is described in Section III-B. For the controlled propagation environment case, we have two hypothetical transmitting antennas. Due to the hardware limitations, we can only simulate one hypothetical receiving antenna at a time, so we simulate the 2×1 channel model twice with the same K value, and then combine the two received signals. More precisely, we correct the signals received by the two antennas separately with the help of the estimated CSI as explained in Section II-B. Then the corrected signals are combined and normalized for detection.

The BER performance in a controlled propagation environment is shown in FIGURE 12. We extract the performance in terms of BER variation concerning E_b/N_0, which represents the energy per bit over the noise power spectral density. In addition, we calculate the real-time SNR by measuring the power in band of the signal and the noise separately to calculate the E_b/N_0. The BER results are given for five different values of Rician K-factor, one corresponds to a scenario nearly without NLOS paths (K = 40 dB) and the others correspond to scenarios with different proportions of NLOS paths. One can remark that the SM system with the proposed CSI estimator performs better for the smaller values of K. From the theoretical point of view, it can be explained by the fact that the difference between the $N_t \times N_r$ values in the channel matrix $\mathbf{H}$ is minimal when the K factor is significant, which makes the antenna detection more difficult.

It should be pointed that the BER performance with the estimated CSI at the simulation level has a performance comparable to the BER performance with the perfect CSI [21]. We can also remark that the experimental results with a controlled propagation environment follow the BER performance of the simulation results in FIGURE 12. The slight degradation may be caused by the nonidealities of the hardware implementation. The RF parts of the transmitting and receiving end are considered to be ideal in the simulation. However, the nonidealities (e.g. IQ imbalance, phase noise, nonlinearity of the PA, etc.) may occur in the experimental case. The impact of the nonidealities on SM system at the simulation level is discussed in [33]. In addition, the noise power spectral density in the simulation was calculated for a temperature of 25°C and that in reality (experimental part) this temperature is not exactly the same.

B. BER PERFORMANCE IN A REALISTIC WIRELESS SCENARIO

The real propagation environment is demonstrated in FIGURE 11. Here, the distance between Tx1 and Tx2 antennas is equal to the distance between Rx1 and Rx2 antennas, which is equal to 3/2 wavelength. The distance is set to facilitate the introduction of the full duplex technique afterwards by placing a second antenna at half wavelength to complete the antenna cancellation of electromagnetic waves [34]. To vary the LOS/NLOS propagation environment, three typical scenarios are introduced:

- Electromagnetic absorbers block the LOS path.
- The absorbers partially block the direct path (LOS).
- No absorber is placed between the TX and the RX antennas.

By using the method described in Section III-B, the characteristics of the propagation environment have been measured. Three representative values of the Rician K-factor are obtained by the channel sounding under these three mixed LOS/NLOS scenarios: $K = 5.3$ dB, 20.1 dB, and 39.1 dB. The measurements reveal that when there are no electromagnetic absorbers and the distance between the transmitting and

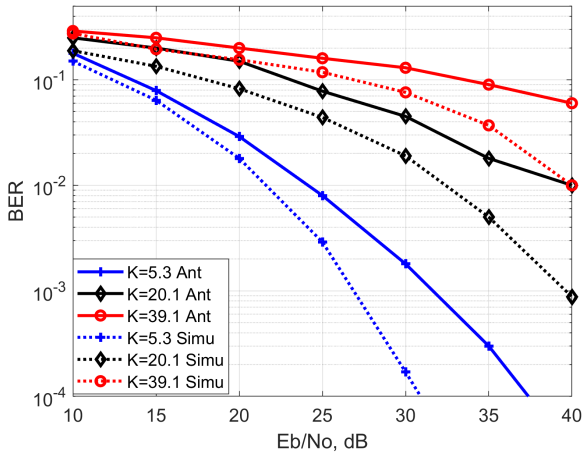

FIGURE 14. BER simulation and experimental results with real propagation environment of the SM system with $N_t = 2$ under three mixed LOS/NLOS scenarios.

receiving antennas is within 3 meters, the K factor can reach nearly 40 dB. This result indicates that the propagation environment is a LOS one. In these three scenarios, the measured average power delays are given in FIGURE 13.

Experimentally, the BER performance under these three mixed LOS/NLOS scenarios is evaluated. The experimental results confronted with the simulation ones are given in FIGURE 14. In the simulation framework, the three Rician K-factor values measured previously are configured. For the three scenarios, a small variation between the simulated and the experimental BER results can be remarked. This gap may be induced by the instability of the propagation channel. Indeed, it is supposed that the channel is slightly varying between the channel sounding step and the actual experimentation steps. Besides, the accuracy of channel sounding can be imperfect because the bandwidth setup is not large enough. This variation is more evident when Eb/N0 has a strong value which may be caused by the accuracy on the BER calculations. Moreover, a better performance in terms of BER may be highlighted when a high diversity propagation channel is employed. Indeed, for a given target of BER, it requires a smaller E_b/N_0 for the smaller K value than the higher K value. Generally, we can conclude that the considered 2×2 SM system can maintain the performance in a real propagation environment, especially in presence of multipath and NLOS conditions.

V. CONCLUSION

In this paper, the performance of a SM system has been analyzed, for the first time, under mixed LOS/NLOS conditions with the help of an experimental framework based on NI VST modules. This study compensated for the lack of experiments on SM systems in realistic propagation channels. The software framework for the generation and the analysis of the SM signals has been presented. In particular, a CSI detector for the channel estimation was designed instead of assuming the availability of the perfect CSI at the receiver. The index of transmitting antenna and symbol are detected respectively by employing a low complexity ML detection method. Moreover, an extensive analysis of the experimental setup was presented and two models of the propagation environments (controlled one and wireless one) were proposed. The case of the controlled propagation environment has the advantage of being configurable, but the multipath model is too simple. Meanwhile, the latter tackled scenario introduces a real indoor channel environment. Since the characteristics of the real wireless channel are unknown, a channel sounding method by using the good correlation property of PN sequences has been employed in order to extract the channel coefficients. As a result, the BER performance of practical implementation for the two proposed propagation environments was analyzed and both followed well the simulation results. Specifically, the performance in terms of BER could be better in presence of multipath and NLOS propagation conditions.

For the directions of future research, it is worth analyzing the compensation of the nonidealities impact on the SM system from the hardware level to improve the system performance. Efforts can also be done on the accuracy of channel sounding and more realistic modulation schemes, paying attention to the balance between the accuracy of the study and the computational cost. More precisely, higher bandwidth is expected to be employed which will make the channel sounding results more accurate and the BER estimation closer to the real values. The composite fading channel models are also envisaged in order to better match with the small signal variation and the diversity of channels. A In addition, the experimental analysis of combining full-duplex radio and SM is also expected, which brings a double spectral efficiency.

REFERENCES

[1] E. Basar, M. Wen, R. Mesleh, M. Di Renzo, Y. Xiao, and H. Haas, "Index modulation techniques for next-generation wireless networks," *IEEE Access*, vol. 5, pp. 16693–16746, 2017.

[2] A. Mohammadi and F. M. Ghannouchi, "Single RF front-end MIMO transceivers," *IEEE Commun. Mag.*, vol. 49, no. 12, pp. 104–109, Dec. 2011.

[3] T. Mao, Q. Wang, and Z. Wang, "Spatial modulation for terahertz communication systems with hardware impairments," *IEEE Trans. Veh. Technol.*, vol. 69, no. 4, pp. 4553–4557, Apr. 2020.

[4] P. Liu, M. Di Renzo, and A. Springer, "Line-of-sight spatial modulation for indoor mmWave communication at 60 GHz," *IEEE Trans. Wireless Commun.*, vol. 15, no. 11, pp. 7373–7389, Nov. 2016.

[5] M. Saad, F. Bader, A. C. Al Ghouwayel, H. Hijazi, N. Bouhel, and J. Palicot, "Generalized spatial modulation for wireless terabits systems under sub-THz channel with RF impairments," in *Proc. IEEE Int. Conf. Acoust., Speech Signal Process. (ICASSP)*, May 2020, pp. 5130–5134.

[6] D. Phan-Huy, Y. Kokar, K. Rachedi, P. Pajusco, A. Mokh, T. Magounaki, R. Masood, C. Buey, P. Ratajczak, N. Malhouroux-Gaffet, J. Conrat, J. Prévotet, A. Ourir, J. De Rosny, and M. D. Renzo, "Single-carrier spatial modulation for the Internet of Things: Design and performance evaluation by using real compact and reconfigurable antennas," *IEEE Access*, vol. 7, pp. 18978–18993, 2019.

[7] M. Wen, B. Zheng, K. J. Kim, M. Di Renzo, T. A. Tsiftsis, K. C. Chen, and N. Al-Dhahir, "A survey on spatial modulation in emerging wireless systems: Research progresses and applications," *IEEE J. Sel. Areas Commun.*, vol. 37, no. 9, pp. 1949–1972, Sep. 2019.

[8] D. N. Viet, M. Di Renzo, V. Basavarajappa, B. B. Exposito, J. Basterrechea, and D.-T. Phan-Huy, "Spatial modulation based on reconfigurable antennas: Performance evaluation by using the prototype of a reconfigurable antenna," *EURASIP J. Wireless Commun. Netw.*, vol. 2019, no. 1, pp. 1–17, Dec. 2019.
[9] M. Di Renzo, H. Haas, A. Ghrayeb, S. Sugiura, and L. Hanzo, "Spatial modulation for generalized MIMO: Challenges, opportunities, and implementation," *Proc. IEEE*, vol. 102, no. 1, pp. 56–103, Jan. 2014.
[10] P. Yang, M. Di Renzo, Y. Xiao, S. Li, and L. Hanzo, "Design guidelines for spatial modulation," *IEEE Commun. Surveys Tuts.*, vol. 17, no. 1, pp. 6–26, 1st Quart., 2015.
[11] J. Jeganathan, A. Ghrayeb, L. Szczecinski, and A. Ceron, "Space shift keying modulation for MIMO channels," *IEEE Trans. Wireless Commun.*, vol. 8, no. 7, pp. 3692–3703, Jul. 2009.
[12] R. Mesleh, S. S. Ikki, and H. M. Aggoune, "Quadrature spatial modulation," *IEEE Trans. Veh. Technol.*, vol. 64, no. 6, pp. 2738–2742, Jun. 2015.
[13] A. Younis, N. Serafimovski, R. Mesleh, and H. Haas, "Generalised spatial modulation," in *Proc. 44th Asilomar Conf. Signals, Syst. Comput.*, Nov. 2010, pp. 1498–1502.
[14] J. Jeganathan, A. Ghrayeb, and L. Szczecinski, "Spatial modulation: Optimal detection and performance analysis," *IEEE Commun. Lett.*, vol. 12, no. 8, pp. 545–547, Aug. 2008.
[15] S. Sugiura and L. Hanzo, "Effects of channel estimation on spatial modulation," *IEEE Signal Process. Lett.*, vol. 19, no. 12, pp. 805–808, Dec. 2012.
[16] E. Basar, Ü. Aygölu, E. Panayirci, and H. V. Poor, "Performance of spatial modulation in the presence of channel estimation errors," *IEEE Commun. Lett.*, vol. 16, no. 2, pp. 176–179, Feb. 2012.
[17] A. Mokh, M. Crussière, and M. Hélard, "Performance analysis of extended RASK under imperfect channel estimation and antenna correlation," in *Proc. IEEE Wireless Commun. Netw. Conf. (WCNC)*, Apr. 2018, pp. 1–6.
[18] A. Afana, N. Abu-Ali, and S. Ikki, "On the joint impact of hardware and channel imperfections on cognitive spatial modulation MIMO systems: Cramér–Rao bound approach," *IEEE Syst. J.*, vol. 13, no. 2, pp. 1250–1261, Jun. 2019.
[19] M. M. Alwakeel, "Quadrature spatial modulation performance analysis over Rician fading channels," *J. Commun.*, vol. 11, no. 3, pp. 249–254, 2016.
[20] H. S. Hussein, M. Elsayed, and U. S. Mohamed, "Fully-quadrature spatial modulation over rician fading channels," in *Proc. Int. Japan-Africa Conf. Electron., Commun. Comput. (JAC-ECC)*, Dec. 2018, pp. 39–42.
[21] Y. Zhou, F. Hutu, and G. Villemaud, "Analysis of a spatial modulation system over time-varying rician fading channel with a CSI detector," in *Proc. IEEE Radio Wireless Symp. (RWS)*, Jan. 2020, pp. 217–220.
[22] A. Younis, W. Thompson, M. Di Renzo, C.-X. Wang, M. A. Beach, H. Haas, and P. M. Grant, "Performance of spatial modulation using measured real-world channels," in *Proc. IEEE 78th Veh. Technol. Conf. (VTC Fall)*, Sep. 2013, pp. 1–5.
[23] N. Serafimovski, A. Younis, R. Mesleh, P. Chambers, M. Di Renzo, C. X. Wang, P. M. Grant, M. A. Beach, and H. Haas, "Practical implementation of spatial modulation," *IEEE Trans. Veh. Technol.*, vol. 62, no. 9, pp. 4511–4523, Nov. 2013.
[24] K. Jiang, Z. Liu, P. Yang, Y. Xiao, and S. Li, "An experimental investigation of enhanced SM-OFDM over indoor rician multipath channels," *IEEE Trans. Veh. Technol.*, vol. 69, no. 2, pp. 2291–2295, Feb. 2020.
[25] O. Hiari, R. Mesleh, S. Alshaer, and F. Shahin, "First hardware implementation of an SSK MIMO system with no RF-chain at the transmitter," *IEEE Trans. Ind. Electron.*, vol. 68, no. 5, pp. 4477–4484, May 2021.
[26] Y. Kokar, K. Rachedi, A. Ourir, J. de Rosny, D.-T. Phan-Huy, J.-C. Prevotet, and M. Helard, "Demo abstract: Spatial modulation based transmission using a reconfigurable antenna," in *Proc. IEEE Conf. Comput. Commun. Workshops (INFOCOM WKSHPS)*, Apr. 2019, pp. 985–986.
[27] National Instruments. *Getting Started Guide NI PXIe-5646R*. Accessed: Mar. 2018. [Online]. Available: https://www.ni.com/pdf/manuals/374316c.pdf
[28] National Instruments. *Getting Started Guide NI RF Signal Generators*. Accessed: Jun. 2018. [Online]. Available: https://zone.ni.com/reference/en-XX/help/371025V-01/rfsg/getting_started/
[29] National Instruments. *Getting Started Guide NI RF Signal Analyzers*. Accessed: Jun. 2018. [Online]. Available: https://zone.ni.com/reference/en-XX/help/372058U-01/nirfsa/getting_started/
[30] H. Men and M. Jin, "A low-complexity ML detection algorithm for spatial modulation systems with M PSK constellation," *IEEE Commun. Lett.*, vol. 18, no. 8, pp. 1375–1378, Aug. 2014.
[31] M. Luo, "Indoor radio propagation modeling for system performance prediction," M.S. thesis, INSA de Lyon, Villeurbanne, France, Jul. 2013. [Online]. Available: https://tel.archives-ouvertes.fr/tel-00937481
[32] R. N. Mutagi, "Pseudo noise sequences for engineers," *IEEE Electron. Commun. Eng. J.*, vol. 8, no. 2, pp. 79–87, Apr. 1996.
[33] Y. Zhou, F. Hutu, and G. Villemaud, "Impact of receiver non-idealities on a full duplex spatial modulation system performance," *IEEE Wireless Commun. Lett.*, vol. 9, no. 12, pp. 2083–2087, Dec. 2020.
[34] J. I. Choi, S. Hong, M. Jain, S. Katti, P. Levis, and J. Mehlman, "Beyond full duplex wireless," in *Proc. 46th Asilomar Conf. Signals, Syst. Comput. (ASILOMAR)*, Nov. 2012, pp. 40–44.

YANNI ZHOU (Associate Member, IEEE) was born in Lianyungang, China, in 1995. She received the B.S. degree in electrical information engineering from Northwestern Polytechnical University (NPU), Xi'an, China, in 2016, and the Engineering degree in electrical engineering from the National Institute of Applied Science (INSA) de Lyon, France, in 2018. She is currently pursuing the Ph.D. degree with the INSA-Lyon/INRIA, France. She is also a member of the INRIA Socrate Team, CITI Laboratory. Her main research interests include RF architectures and system level simulation, spatial modulation systems, full-duplex systems, radio propagation, and measurements.

FLORIN DORU HUTU (Senior Member, IEEE) was born in Iaşi, Romania, in 1979. He received the Engineering degree in electronics and telecommunications and the master's degree in digital radio-communications from the Faculty of Electronics, Telecommunications and Information Technology, Gheorghe Asachi Technical University of Iasi, in 2003 and 2004, respectively, and the Ph.D. degree in automatic control from the University of Poitiers, France, in 2007. After two years of a postdoctoral position with the XLIM Laboratory, in September 2010, he became an Associate Professor with INSA Lyon, France. He joined the INSA Lyon's Electrical Engineering Department and the INRIA's Socrate Team, CITI Laboratory. He is also involved in the design of software-defined radio architectures for the IoT. He is the author of more than 70 national and international scientific articles. His research interests include energy efficient radio communications (wake-up radio, energy harvesting, and wireless power transfer) and RFID technologies.

GUILLAUME VILLEMAUD (Senior Member, IEEE) received the M.S. degree in electrical engineering from the University of Limoges, Limoges, France, in 1999, and the Ph.D. degree in electronics, in 2002. From 1999 to 2002, he worked at IRCOM, Limoges, on compact integrated antennas. From 2002 to 2003, he developed multi-band hybrid arrays for mobile phone localization for CREAPE, and then joined the CITI Laboratory, Lyon, France, in 2003. He is currently an Associate Professor at INSA Lyon, France, the Head of the International Exchange Office of the Electrical Engineering Department, and a member of the Executive Committee. He is the Site Leader of the FP7 Project iPlan for the development of planning and optimization tools for the deployment of Femtocells, also responsible of the Flexible radio terminals' axis of the INRIA SOCRATE team. He is also strongly involved in the development of the Cognitive Radio Platform, part of the Future Internet-of-Things equipment of excellence funded by the French Government. He has published more than 100 international technical papers. His research interests include antenna design and integration, antenna diversity and multiple antenna processing (SIMO, MIMO), and system level simulation, coverage prediction, radio propagation, and measurements.